ACS OMEGA

Open Access
This article is licensed under CC-BY-NC-ND 4.0

http://pubs.acs.org/journal/acsodf
Article

Deep Ultraviolet Optical Anisotropy of β-Gallium Oxide Thin Films

Yu-Che Ho, Gaihua Ye, Cynthia Nnokwe, Vladimir Kuryatkov, Juliusz Warzywoda, Luis Grave de Peralta, Rui He,* and Ayrton Bernussi*

Cite This: *ACS Omega* 2024, 9, 27963−27968

Read Online

ACCESS | Metrics & More | Article Recommendations

ABSTRACT: β-Crystalline phase gallium oxide (β-Ga_2O_3) is an ultrawide bandgap material with prospective applications in electronics and deep ultraviolet (DUV) optoelectronics and optics. The monoclinic crystal structure of β-Ga_2O_3 results in optical anisotropy to incident light with different polarization states. This attribute can lead to different optical applications in the DUV. In this article, we investigated the optical properties of β-Ga_2O_3 thin films grown by pulsed laser deposition technique on sapphire substrates with different crystallographic orientations. Marked in-plane polarization anisotropy, determined by reflectance and Raman spectroscopy, was observed for β-Ga_2O_3 films deposited on an *r*-cut sapphire substrate. In contrast, isotropic optical properties were observed in β-Ga_2O_3 films deposited on a *c*-cut sapphire substrate.

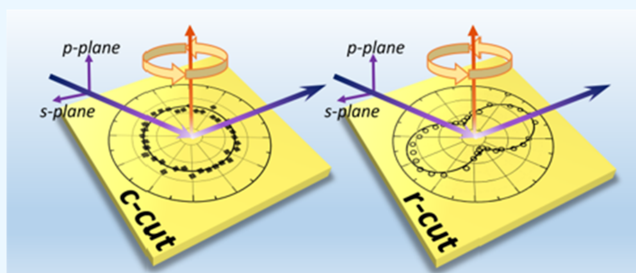

1. INTRODUCTION

Gallium oxide (Ga_2O_3) has gained increased attention in the past few years due to its potential application in high-power electronics, optoelectronics, and radiofrequency (RF).[1−4] Ga_2O_3 is an ultrawide bandgap material with high thermal stability, excellent chemical and mechanical properties, and breakdown field strength as large as 8 MV/cm,[5] making this material suitable for high-voltage and high-temperature applications.[6] Additionally, Ga_2O_3 can be realized in several crystalline phases, including corundum (α), defective spinel (γ), cube (δ), orthorhombic (ε), and monoclinic (β) Ga_2O_3, each with its own unique properties for a broad range of applications.[7] β-Ga_2O_3, which is typically achieved under high growth temperatures (>700 °C), is the most studied crystalline phase and has unique optical properties that makes it attractive for various optoelectronic applications. β-Ga_2O_3 has a bandgap of ∼4.8 eV, making it also an excellent candidate for deep UV (DUV) photodetectors.

Monoclinic β-Ga_2O_3 has lattice constants a = 12.214 Å, b = 3.0371 Å, c = 5.7981 Å, and β = 103.83°,[8,9] and this results in anisotropic optical polarization near the DUV bandgap energy. Bulk and thin films β-Ga_2O_3 have been grown using different methods[10−14] and deposition techniques.[15−23] However, the optical anisotropy of β-Ga_2O_3 has been only investigated in bulk single-crystal β-Ga_2O_3.[24,25] The DUV optical anisotropy of β-Ga_2O_3 thin films remains largely unexplored.

In the present study, we report DUV-polarized reflectance and -polarized Raman spectroscopy measurements of β-Ga_2O_3 thin films deposited on $(10\bar{1}2)$ *r*-cut sapphire substrates (*r*-cut for short) and (0001) *c*-cut sapphire substrates (*c*-cut for short). Markedly in-plane DUV optical anisotropy was observed for β-Ga_2O_3 films grown on *r*-cut sapphire substrates by using both optical techniques. Measured DUV-polarized reflectance spectra of β-Ga_2O_3 thin films deposited on *r*-cut are in good agreement with simulations using the rigorous coupled wave analysis (RCWA) technique.

2. EXPERIMENTS

β-Ga_2O_3 films (∼275 nm thick) were simultaneously deposited on *c*- and *r*-cut sapphire substrates by using the pulsed laser deposition (PLD) technique. Before the deposition, the substrates were sonicated in acetone, isopropyl alcohol, deionized water, and then breezed with nitrogen gas. The samples were deposited at 750 °C growth temperature with an initial growth chamber pressure <10^{-9} Torr. During the deposition, an O_2 flow rate of 2 sccm and 25 mTorr chamber pressure were kept constant. A sintered β-Ga_2O_3 target was ablated using the 249 nm wavelength of the KrF excimer laser with a fluency and repetition rate of 2.4 J/cm^2 and 10 Hz, respectively.

All fabricated samples were characterized by polarized Raman spectroscopy, high-resolution X-ray diffraction (HRXRD), scanning electron microscopy (SEM), and polarized DUV reflectance and ellipsometry spectroscopy.

Received: December 22, 2023
Revised: April 25, 2024
Accepted: June 11, 2024
Published: June 21, 2024

© 2024 The Authors. Published by American Chemical Society

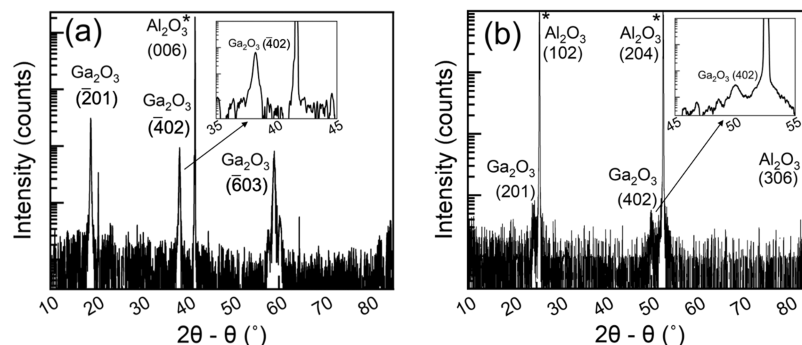

Figure 1. HRXRD $2\theta-\theta$ scans of the (a) β-Ga_2O_3/*c*-cut and (b) β-Ga_2O_3/*r*-cut. The insets show a zoom-in of the peaks at ($\bar{4}$02) (a) and (402) (b).

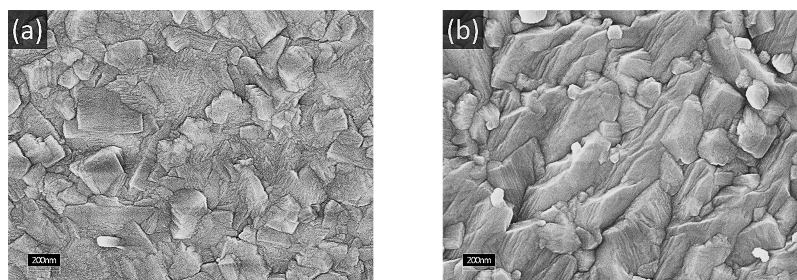

Figure 2. SEM images of the (a) β-Ga_2O_3/*c*-cut and (b) β-Ga_2O_3/*r*-cut.

DUV-polarized reflectance and ellipsometry were performed using the polarized light from a xenon lamp source illuminating the samples at fixed incident angle θ = 70° (using a Horiba Jobin Yvon UVISEL Ellipsometer) with an elliptical spot at the sample surface with major and minor axis lengths of ~3 and ~1 mm, respectively. Reflectance and Raman measurements were carried out by rotating the samples' azimuth angle φ from 0° to 360°. The polarized reflectance spectra results were compared with the simulated RCWA ones.

Angle-resolved Raman measurements were carried out at room temperature using a linearly polarized 532 nm excitation laser in backscattering geometry. A 100× objective lens was used, and the laser light was focused to a spot size of ~1 μm. The laser power was kept at ~10 mW. The scattered light was dispersed by a Horiba LabRAM HR800 Confocal Raman Microscope system and detected by a thermoelectrically cooled CCD (charge-coupled device) camera. The β-Ga_2O_3 *r*-cut and *c*-cut samples were mounted on a rotatable stage and measured at every 10° angle.

3. RESULTS AND DISCUSSION

Figure 1a,b shows the HRXRD diffraction patterns of the β-Ga_2O_3/*c*-cut and β-Ga_2O_3/*r*-cut thin films, respectively. The peaks centered at 18.8°, 38.3° and 59.0° in Figure 1a correspond to, respectively, the ($\bar{2}$01), ($\bar{4}$02), ($\bar{6}$03) diffractions of a β-Ga_2O_3 crystalline phase.[26−31] The peak centered at 41.5° corresponds to the diffraction of the *c*-cut sapphire substrate. In Figure 1b, the peaks centered at 25.6° and 52.5° correspond to the *r*-cut sapphire substrate. The relatively low intensity peaks centered at 24.5° and 49.9° correspond to the (201) and (402) diffractions, respectively, of the β-Ga_2O_3 film. We determined the full width at half-maximum (fwhm) of the β-Ga_2O_3 diffraction peaks at ($\bar{4}$02) and (402) as 0.206° and 0.884°, respectively, for the *c*-cut and *r*-cut samples. The wider diffraction pattern peaks of the β-Ga_2O_3/*r*-cut suggests the crystalline grains were arranged with a higher mosaicity, when compared to the *c*-cut, or the ($\bar{4}$02) direction of the β-Ga_2O_3 crystal orientation does not align with the *r*-cut plane.[32−38]

Figure 2a,b shows representative top view SEM images of the β-Ga_2O_3/*c*-cut and β-Ga_2O_3/*r*-cut, respectively. The images revealed a granular morphology with no apparent voids between adjacent grains on both samples.[36,39,40] We determined average lateral grain sizes of ~193 and ~400 nm for the β-Ga_2O_3 films deposited on *c*-cut and *r*-cut sapphire substrates, respectively.

The optical reflectance anisotropy of the β-Ga_2O_3 samples was investigated using the polarized measurement setup schematically illustrated in Figure 3. *p*-Polarized or *s*-polarized light illuminates the samples at a fixed angle of θ = 70°. Reflectance measurements (R_p or R_s) were performed by rotating the samples in the $x-y$ plane (azimuth angle $0 \leq \varphi \leq 360°$). The same configuration was also used in the spectroscopic ellipsometry measurements.

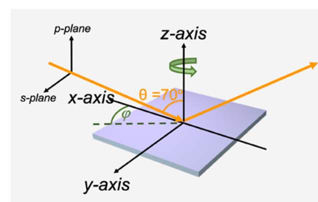

Figure 3. Polarized reflectance spectroscopy measurement.

Measured DUV R_p and R_s spectra of β-Ga_2O_3/*r*-cut at φ = 0° are shown, respectively, in Figure 4a,b. Below the Ga_2O_3 bandgap energy (4.8 eV or 253 nm), the spectra show periodic oscillations due to the constructive/destructive interference between the film and the substrate. The peak/valley position wavelengths of the oscillations shown in Figure 4 are in good

https://doi.org/10.1021/acsomega.3c10280
ACS Omega 2024, 9, 27963−27968

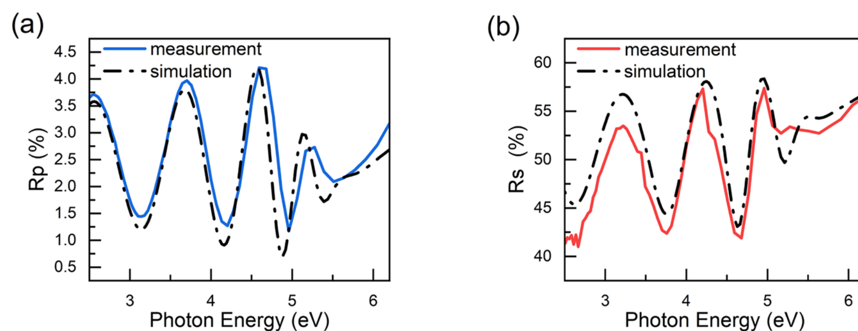

Figure 4. Measured and simulated polarized reflectance spectra of β-Ga_2O_3/*r*-cut at $\varphi = 0°$: (a) *p*-polarization and (b) *s*-polarization.

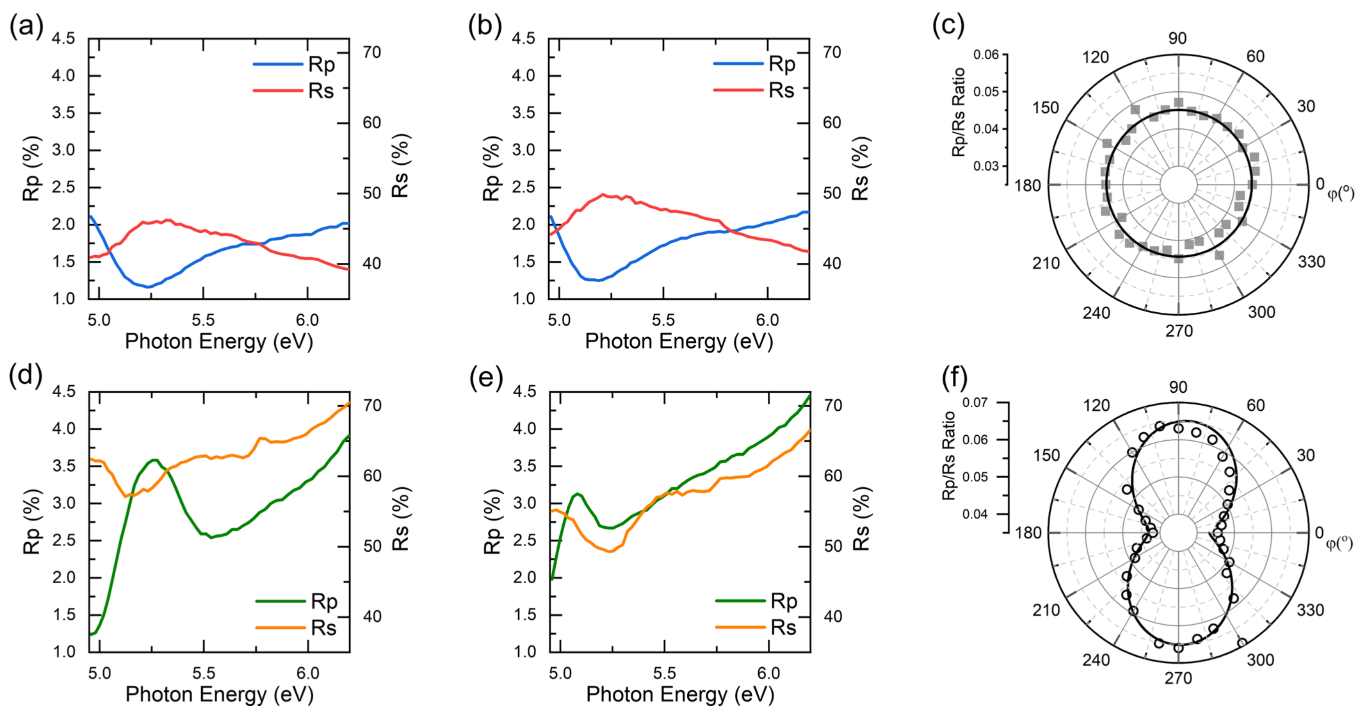

Figure 5. *p*- and *s*-polarized reflectance spectra and R_p/R_s ratio polar plots (at $\lambda = 210$ nm or $E \sim 5.9$ eV). β-Ga_2O_3/*c*-cut: (a) $\varphi = 0°$, (b) $\varphi = 90°$ and (c) R_p/R_s polar plots; β-Ga_2O_3/*r*-cut: (d) $\varphi = 0°$, (e) $\varphi = 90°$, and (f) R_p/R_s polar plots. The solid lines in (c) and (f) are guides for the eyes.

correspondence with those calculated using the Fresnel Equations with an incident angle of $\theta = 70°$ (see Figure 3). In addition, the notable difference in reflectance between R_p (Figure 4a) and R_s (Figure 4b) is attributed to the large incident angle ($\theta = 70°$), which is close to the film's Brewster angle. We verified small changes in the DUV R_p and R_s spectra of β-Ga_2O_3 (for both *r*- and *c*-cut) due to thickness and roughness variations across the sample. However, the ratio R_p/R_s remained nearly uniform.

Complementary spectroscopic ellipsometry (SE) measurements (not shown here) were performed to determine the wavelength-dependent complex refractive index of the Ga_2O_3 samples at different azimuthal angles. The obtained refractive indices determined from the SE experiments were used in the simulation of R_s and R_p by using the RCWA method. A multilayer model consisting of the sapphire substrate, the β-Ga_2O_3 film, and a thin top layer mimicking the sample surface roughness (a 50%/50% mix of air/Ga_2O_3) was used in those simulations. The simulated R_s and R_p spectra for a β-Ga_2O_3/*r*-cut sample for $\varphi = 0°$ are also shown in Figure 4a,b, respectively. A good agreement between simulated and measured R_s and R_p is clearly visible in Figure 4, indicating that the RCWA method can be effectively used to model the optical anisotropy of β-Ga_2O_3 films in the DUV.

To verify the optical anisotropy of the β-Ga_2O_3 samples, we measured the R_s and R_p spectra in the DUV at $\varphi = 0°$ and $\varphi = 90°$ as shown in Figure 5a,b and d,e. The reflectance spectra for the β-Ga_2O_3/*c*-cut sample at $\varphi = 0°$ (Figure 5a) and $\varphi = 90°$ (Figure 5b) are nearly identical. In contrast, the reflectance spectra of the β-Ga_2O_3/*r*-cut sample are very different for $\varphi = 0°$ (Figure 5d) and for $\varphi = 90°$ (Figure 5e). The results shown in Figure 5 reveal a marked optical anisotropy for the β-Ga_2O_3/*r*-cut sample. To further confirm the DUV optical anisotropy of the β-Ga_2O_3/*r*-cut sample, we show in Figure 5c,f, respectively, the polar plots ($0 \leq \varphi \leq 360°$) of the ratio R_p/R_s (at $\lambda = 210$ nm or $E = 5.9$ eV) for the β-Ga_2O_3/*c*-cut and β-Ga_2O_3/*r*-cut samples. The ratio R_p/R_s was used to minimize possible fluctuations in the DUV reflectivity amplitude during the measurements.[41,42] The R_p/R_s polar plot for the β-Ga_2O_3/*c*-cut sample showed a nearly circular dependence with the azimuthal angle φ (Figure 5c). Conversely, the R_p/R_s polar plot for the β-Ga_2O_3/*r*-cut sample exhibited a two-lobed symmetry, confirming the optical anisotropy for this sample in

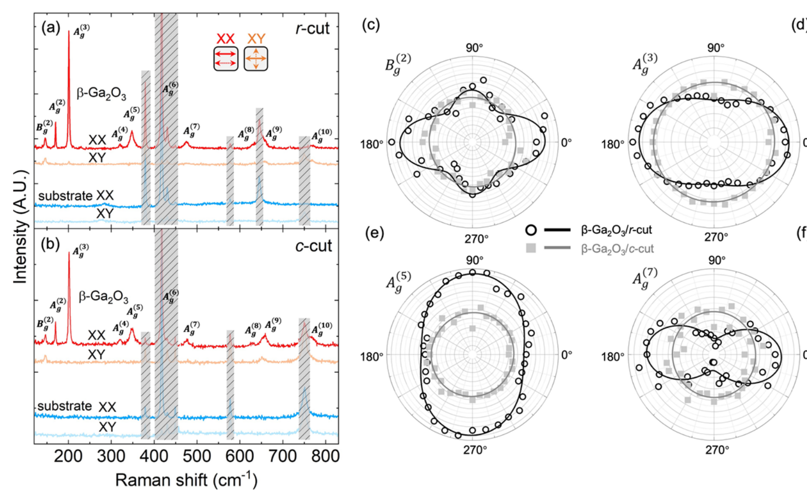

Figure 6. (a) Linearly polarized Raman spectra from the β-Ga_2O_3/*r*-cut sample. *XX* and *XY* refer to the linearly parallel and crossed polarization configuration, respectively, in the laboratory coordinate system, not the sample coordinate system. Spectra from the substrates are included for comparison, and the modes from the substrate are shaded with gray stripes. (b) Same as (a) for the β-Ga_2O_3/*c*-cut sample. (c−f) Rotational angle dependence of area intensities of $B_g^{(2)}$, $A_g^{(3)}$, $A_g^{(5)}$, and $A_g^{(7)}$ modes from both β-Ga_2O_3/*r*-cut and β-Ga_2O_3/*c*-cut samples in the *XX* polarization configuration. The solid lines in panels c−f are guides to the eye. All Raman data were taken at room temperature by using 532 nm laser light.

which distinct R_p/R_s values can be clearly verified for $\varphi = 90°$ (and $\varphi = 270°$) and $\varphi = 0°$ (and $\varphi = 180°$).

The optical anisotropy of the β-Ga_2O_3/*r*-cut sample was also revealed in angle-resolved Raman spectroscopy measurement. Figure 6a,b show the Raman spectra taken in linearly parallel (*XX*) and linearly crossed (*XY*) channels from β-Ga_2O_3/*r*-cut and β-Ga_2O_3/*c*-cut samples, respectively. Spectra from the respective substrates are also included for comparison, and the modes from the substrate are shaded in gray stripes. β-Ga_2O_3 has 15 Raman-active modes, including 10 A_g symmetry modes and 5 B_g symmetry modes.[43] Raman lines below 120 cm^{-1} ($A_g^{(1)}$ and $B_g^{(1)}$) were obscured by signals from the air, and thus, we focus on modes with frequencies higher than 120 cm^{-1}. In the spectra from both β-Ga_2O_3/*r*-cut and β-Ga_2O_3/*c*-cut samples shown in Figure 6a,b, nine A_g modes (from $A_g^{(2)}$ to $A_g^{(10)}$) are observed in the linearly parallel channel. However, the $A_g^{(6)}$, $A_g^{(8)}$, $A_g^{(9)}$, and $A_g^{(10)}$ modes from the β-Ga_2O_3/*r*-cut sample and $A_g^{(6)}$ and $A_g^{(10)}$ modes from β-Ga_2O_3/*c*-cut overlap or are spectrally very close to the Raman lines from the substrate. The A_g modes overall are very weak and barely observed in the linearly crossed channel. Because our laser light polarization and the direction of laser propagation are not aligned with the principal axes of the samples, B_g modes could also be observed in principle. A well-defined $B_g^{(2)}$ mode was seen in both linearly parallel and crossed channels. Higher-frequency B_g modes, $B_g^{(3)}$, $B_g^{(4)}$, and $B_g^{(5)}$, are not observed possibly because their intensities are relatively weak, and they are spectrally close to A_g modes. We performed angle-resolved Raman measurements in which we fixed the polarizations of incident and selected scattered light and rotated the sample in the *x*−*y* plane, and then we plotted intensities of selected well-defined Raman modes as a function of the rotational angle φ. Figure 6c−f show the parallel (*XX*) channel angle dependence of Raman intensities of $B_g^{(2)}$, $A_g^{(3)}$, $A_g^{(5)}$, and $A_g^{(7)}$ modes from both β-Ga_2O_3/*r*-cut and β-Ga_2O_3/*c*-cut samples. It is seen that the β-Ga_2O_3/*r*-cut sample shows anisotropy, whereas the β-Ga_2O_3/*c*-cut sample is isotropic, which agrees well with the results found in reflectance measurements as shown in Figure 5.

The origin of the DUV polarization anisotropy of the β-Ga_2O_3/*r*-cut can be associated with the crystalline arrangement in the film. The XRD observations in Figure 1 support the hypothesis that the β-Ga_2O_3/*r*-cut sample has a larger mosaicity degree and the crystalline orientation of the grains are not aligned with the surface of the *r*-cut sapphire substrate. Instead, the $(\bar{2}01)$ plane of β-Ga_2O_3 are aligned with the (113) or $(2\bar{1}3)$ plane of the *r*-cut sapphire substrate.[34−37] This corresponds to a 3-fold symmetry arrangement of the β-Ga_2O_3 $(\bar{2}01)$ plane rotated at every 120° angle on two of the (113) or $(2\bar{1}3)$ planes of the sapphire substrate, which are inclined by ±27° from the *r*-cut plane.[34] DUV reflectance and Raman mode anisotropy of the β-Ga_2O_3/*r*-cut shown in Figures 5 and 6 are due to the $(\bar{2}01)$ β-Ga_2O_3 crystal tilted arrangement with the (113) or $(2\bar{1}3)$ sapphire substrate orientations.[34,35] On the other hand, the β-Ga_2O_3/*c*-cut crystalline orientation is aligned with the sapphire *c*-cut plane resulting in an isotropic DUV reflectance and Raman mode.

4. CONCLUSIONS

We investigated the optical anisotropy of β-Ga_2O_3 films deposited by the PLD technique on different sapphire substrates. Polarized Raman and DUV reflectance spectroscopy revealed pronounced in-plane optical anisotropy for the β-Ga_2O_3/*r*-cut films. In contrast, β-Ga_2O_3/*c*-cut films showed an isotropic optical response due to the alignment of the grains with the *c*-cut plane. The crystallographic orientation of the grains in the β-Ga_2O_3/*r*-cut films, which is tilted away from the *r*-cut plane, is the underlying origin for the observed optical anisotropy in these samples. The results obtained here can be prospectively important in the development of polarization-dependent optical and optoelectronic devices operating in the DUV.

■ AUTHOR INFORMATION

Corresponding Authors

Rui He − *Electrical and Computer Engineering, Texas Tech University, Lubbock, Texas 79409, United States;* orcid.org/0000-0002-2368-7269; Email: rui.he@ttu.edu

https://doi.org/10.1021/acsomega.3c10280
ACS Omega 2024, 9, 27963−27968

Ayrton Bernussi − *Electrical and Computer Engineering and Nano Tech Center, Texas Tech University, Lubbock, Texas 79409, United States*; Email: Ayrton.Bernussi@ttu.edu

Authors

Yu-Che Ho − *Electrical and Computer Engineering and Nano Tech Center, Texas Tech University, Lubbock, Texas 79409, United States*; orcid.org/0009-0003-1536-6435

Gaihua Ye − *Electrical and Computer Engineering, Texas Tech University, Lubbock, Texas 79409, United States*

Cynthia Nnokwe − *Electrical and Computer Engineering, Texas Tech University, Lubbock, Texas 79409, United States*

Vladimir Kuryatkov − *Electrical and Computer Engineering and Nano Tech Center, Texas Tech University, Lubbock, Texas 79409, United States*

Juliusz Warzywoda − *Materials Characterization Center, Texas Tech University, Lubbock, Texas 79409, United States*

Luis Grave de Peralta − *Nano Tech Center and Department of Physics and Astronomy, Texas Tech University, Lubbock, Texas 79409, United States*

Complete contact information is available at:
https://pubs.acs.org/10.1021/acsomega.3c10280

Notes

The authors declare no competing financial interest.

■ ACKNOWLEDGMENTS

G.Y., C.N., and R.H. are supported by NSF grants nos. DMR-2104036 and DMR-2300640.

■ REFERENCES

(1) Higashiwaki, M.; Sasaki, K.; Kuramata, A.; Masui, T.; Yamakoshi, S. Gallium oxide (Ga2O3) metal-semiconductor field-effect transistors on single-crystal β-Ga2O3 (010) substrates. *Appl. Phys. Lett.* **2012**, *100* (1), No. 013504.

(2) Tippins, H. H. Optical Absorption and Photoconductivity in the Band Edge of β-Ga2O3. *Phys. Rev.* **1965**, *140* (1A), A316−A319.

(3) Tsao, J. Y.; Chowdhury, S.; Hollis, M. A.; Jena, D.; Johnson, N. M.; Jones, K. A.; Kaplar, R. J.; Rajan, S.; Van de walle, C. G.; Bellotti, E.; Chua, C. L.; Collazo, R.; Coltrin, M. E.; Cooper, J. A.; Evans, K. R.; Graham, S.; Grotjohn, T. A.; Heller, E. R.; Higashiwaki, M.; Islam, M. S.; Juodawlkis, P. W.; Khan, M. A.; Koehler, A. D.; Leach, J. H.; Mishra, U. K.; Nemanich, R. J.; Pilawa-podgurski, R. C. N.; Shealy, J. B.; Sitar, Z.; Tadjer, M. J.; Witulski, A. F.; Wraback, M.; Simmons, J. A. Ultrawide-Bandgap Semiconductors: Research Opportunities and Challenges. *Adv. Electron. Mater.* **2018**, *4* (1), No. 1600501.

(4) Onuma, T.; Saito, S.; Sasaki, K.; Masui, T.; Yamaguchi, T.; Honda, T.; Higashiwaki, M. Valence band ordering in β-Ga2O3 studied by polarized transmittance and reflectance spectroscopy. *Jpn. J. Appl. Phys.* **2015**, *54* (11), No. 112601.

(5) He, H.; Orlando, R.; Blanco, M. A.; Pandey, R.; Amzallag, E.; Baraille, I.; Rérat, M. First-principles study of the structural, electronic, and optical properties of Ga2O3 in its monoclinic and hexagonal phases. *Phys. Rev. B* **2006**, *74* (19), No. 195123.

(6) Mastro, M. A.; Kuramata, A.; Calkins, J.; Kim, J.; Ren, F.; Pearton, S. J. Perspective—Opportunities and Future Directions for Ga2O3. *ECS Journal of Solid State Science and Technology* **2017**, *6* (5), P356.

(7) Pearton, S. J.; Yang, J.; Cary, P. H., IV; Ren, F.; Kim, J.; Tadjer, M. J.; Mastro, M. A. A review of Ga2O3 materials, processing, and devices. *Appl. Phys. Rev.* **2018**, *5* (1), No. 011301.

(8) Geller, S. Crystal structure of β-Ga2O3. *J. Chem. Phys.* **1960**, *33* (3), 676−684.

(9) Åhman, J.; Svensson, G.; Albertsson, J. A reinvestigation of β-gallium oxide, Acta Crystallographica Section C: Crystal Structure. *Communications* **1996**, *52* (6), 1336−1338.

(10) Galazka, Z.; Uecker, R.; Irmscher, K.; Albrecht, M.; Klimm, D.; Pietsch, M.; Brützam, M.; Bertram, R.; Ganschow, S.; Fornari, R. Czochralski growth and characterization of β-Ga2O3 single crystals. *Crystal Research and Technology* **2010**, *45* (12), 1229−1236.

(11) Irmscher, K.; Galazka, Z.; Pietsch, M.; Uecker, R.; Fornari, R. Electrical properties of β-Ga2O3 single crystals grown by the Czochralski method. *J. Appl. Phys.* **2011**, *110* (6), No. 063720.

(12) Kuramata, A.; Koshi, K.; Watanabe, S.; Yamaoka, Y.; Masui, T.; Yamakoshi, S. High-quality β-Ga2O3 single crystals grown by edge-defined film-fed growth. *Jpn. J. Appl. Phys.* **2016**, *55* (12), 1202A2.

(13) Galazka, Z.; Irmscher, K.; Uecker, R.; Bertram, R.; Pietsch, M.; Kwasniewski, A.; Naumann, M.; Schulz, T.; Schewski, R.; Klimm, D.; Bickermann, M. On the bulk β-Ga2O3 single crystals grown by the Czochralski method. *J. Cryst. Growth* **2014**, *404*, 184−191.

(14) Galazka, Z.; Uecker, R.; Klimm, D.; Irmscher, K.; Naumann, M.; Pietsch, M.; Kwasniewski, A.; Bertram, R.; Ganschow, S.; Bickermann, M. Scaling-Up of Bulk β-Ga2O3 Single Crystals by the Czochralski Method. *ECS Journal of Solid State Science and Technology* **2017**, *6* (2), Q3007.

(15) Müller, S.; Von wenckstern, H.; Splith, D.; Schmidt, F.; Grundmann, M. Control of the conductivity of Si-doped β-Ga2O3 thin films via growth temperature and pressure. *physica status solidi (a)* **2014**, *211* (1), 34−39.

(16) Alema, F.; Hertog, B.; Osinsky, A.; Mukhopadhyay, P.; Toporkov, M.; Schoenfeld, W. V. Fast growth rate of epitaxial β−Ga2O3 by close coupled showerhead MOCVD. *J. Cryst. Growth* **2017**, *475*, 77−82.

(17) Ghose, S.; Rahman, S.; Hong, L.; Rojas-ramirez, J. S.; Jin, H.; Park, K.; Klie, R.; Droopad, R. Growth and characterization of β-Ga2O3 thin films by molecular beam epitaxy for deep-UV photodetectors. *J. Appl. Phys.* **2017**, *122* (9), No. 095302.

(18) Sasaki, K.; Higashiwaki, M.; Kuramata, A.; Masui, T.; Yamakoshi, S. MBE grown Ga2O3 and its power device applications. *J. Cryst. Growth* **2013**, *378*, 591−595.

(19) Orita, M.; Hiramatsu, H.; Ohta, H.; Hirano, M.; Hosono, H. Preparation of highly conductive, deep ultraviolet transparent β-Ga2O3 thin film at low deposition temperatures. *Thin Solid Films* **2002**, *411* (1), 134−139.

(20) Baldini, M.; Albrecht, M.; Fiedler, A.; Irmscher, K.; Klimm, D.; Schewski, R.; Wagner, G. Semiconducting Sn-doped β-Ga2O3 homoepitaxial layers grown by metal organic vapour-phase epitaxy. *J. Mater. Sci.* **2016**, *51* (7), 3650−3656.

(21) Gogova, D.; Wagner, G.; Baldini, M.; Schmidbauer, M.; Irmscher, K.; Schewski, R.; Galazka, Z.; Albrecht, M.; Fornari, R. Structural properties of Si-doped β-Ga2O3 layers grown by MOVPE. *J. Cryst. Growth* **2014**, *401*, 665−669.

(22) Garten, L. M.; Zakutayev, A.; Perkins, J. D.; Gorman, B. P.; Ndione, P. F.; Ginley, D. S. Structure property relationships in gallium oxide thin films grown by pulsed laser deposition. *MRS Commun.* **2016**, *6* (4), 348−353.

(23) Okumura, H.; Kita, M.; Sasaki, K.; Kuramata, A.; Higashiwaki, M.; Speck, J. S. Systematic investigation of the growth rate of β-Ga2O3(010) by plasma-assisted molecular beam epitaxy. *Applied Physics Express* **2014**, *7* (9), No. 095501.

(24) Mu, W.; Chen, X.; He, G.; Jia, Z.; Ye, J.; Fu, B.; Zhang, J.; Ding, S.; Tao, X. Anisotropy and in-plane polarization of low-symmetrical β-Ga2O3 single crystal in the deep ultraviolet band. *Appl. Surf. Sci.* **2020**, *527*, No. 146648.

(25) Ueda, N.; Hosono, H.; Waseda, R.; Kawazoe, H. Anisotropy of electrical and optical properties in β-Ga2O3 single crystals. *Appl. Phys. Lett.* **1997**, *71* (7), 933−935.

(26) Seiler, W.; Selmane, M.; Abdelouhadi, K.; Perrière, J. Epitaxial growth of gallium oxide films on c-cut sapphire substrate. *Thin Solid Films* **2015**, *589*, 556−562.

(27) Leedy, K.D.; Chabak, K.D.; Vasilyev, V.; Look, D.C.; Boeckl, J.J.; Brown, J.L.; Tetlak, S.E.; Green, A.J.; Moser, N.A.; Crespo, A.; Thomson, D.B.; Fitch, R.C.; Mccandless, J.P.; Jessen, G.H. Highly conductive homoepitaxial Si-doped Ga2O3 films on (010) β-Ga2O3

by pulsed laser deposition. *Appl. Phys. Lett.* **2017**, *111* (1), No. 012103.
(28) Yu, F.-P.; Ou, S.-L.; Wuu, D.-S. Pulsed laser deposition of gallium oxide films for high performance solar-blind photodetectors. *Opt. Mater. Express* **2015**, *5* (5), 1240−1249.
(29) Oshima, T.; Okuno, T.; Fujita, S. Ga2O3 Thin Film Growth on c-Plane Sapphire Substrates by Molecular Beam Epitaxy for Deep-Ultraviolet Photodetectors. *Jpn. J. Appl. Phys.* **2007**, *46* (11R), 7217.
(30) Chen, Y.; Liang, H.; Xia, X.; Tao, P.; Shen, R.; Liu, Y.; Feng, Y.; Zheng, Y.; Li, X.; Du, G. The lattice distortion of β-Ga2O3 film grown on c-plane sapphire. *Journal of Materials Science: Materials in Electronics* **2015**, *26* (5), 3231−3235.
(31) Li, Y.; Xiu, X.; Xu, W.; Zhang, L.; Xie, Z.; Tao, T.; Chen, P.; Liu, B.; Zhang, R.; Zheng, Y. Microstructural analysis of heteroepitaxial β-Ga2O3 films grown on (0001) sapphire by halide vapor phase epitaxy. *J. Phys. D: Appl. Phys.* **2021**, *54* (1), No. 014003.
(32) Kracht, M.; Karg, A.; Feneberg, M.; Bläsing, J.; Schörmann, J.; Goldhahn, R.; Eickhoff, M. Anisotropic Optical Properties of Metastable (0112) α-Ga2O3 Grown by Plasma-Assisted Molecular Beam Epitaxy. *Physical Review Applied* **2018**, *10* (2), No. 024047.
(33) Jinno, R.; Chang, C. S.; Onuma, T.; Cho, Y.; Ho, S.-T.; Rowe, D.; Cao, M. C.; Lee, K.; Protasenko, V.; Schlom, D. G.; Muller, D. A.; Xing, H. G.; Jena, D. Crystal orientation dictated epitaxy of ultrawide-bandgap 5.4- to 8.6-eV (AlGa)2O3 on m-plane sapphire. *Sci. Adv.* **2021**, *7* (2), No. eabd5891.
(34) Nakagomi, S.; Kaneko, S.; Kokubun, Y. Crystal orientations of β-Ga2O3 thin films formed on m-plane and r-plane sapphire substrates. *physica status solidi (b)* **2015**, *252* (3), 612−620.
(35) Nakagomi, S.; Kaneko, S.; Kokubun, Y. Crystal orientations of β-Ga2O3 thin films formed on n-plane sapphire substrates. *physica status solidi (b)* **2015**, *252* (9), 2117−2122.
(36) Gottschalch, V.; Mergenthaler, K.; Wagner, G.; Bauer, J.; Paetzelt, H.; Sturm, C.; Teschner, U. Growth of β-Ga2O3 on Al2O3 and GaAs using metal-organic vapor-phase epitaxy. *physica status solidi (a)* **2009**, *206* (2), 243−249.
(37) Teherani, F.; Rogers, D.J.; Sandana, V.E.; Bove, P.; Ton-that, C.; Lem, L. L. C.; Chikoidze, E.; Neumann-spallart, M.; Dumont, Y.; Huynh, T.H.; Phillips, M.R.; Chapon, P.; Mcclintock, R.; Razeghi, M. A study into the impact of sapphire substrate orientation on the properties of nominally-undoped β-Ga2O3 thin films grown by pulsed laser deposition. *OPTO* **2017**.
(38) Liu, X.; Liu, Q.; Zhao, B.; Ren, Y.; Tao, B. W.; Zhang, W. L. Comparison of β-Ga2O3 thin films grown on r-plane and c-plane sapphire substrates. *Vacuum* **2020**, *178*, No. 109435.
(39) Nikolaev, V. I.; Maslov, V.; Stepanov, S. I.; Pechnikov, A. I.; Krymov, V.; Nikitina, I. P.; Guzilova, L. I.; Bougrov, V. E.; Romanov, A. E. Growth and characterization of β-Ga2O3 crystals. *J. Cryst. Growth* **2017**, *457*, 132−136.
(40) Rafique, S.; Han, L.; Zhao, H. Synthesis of wide bandgap Ga2O3 (Eg ∼ 4.6−4.7 eV) thin films on sapphire by low pressure chemical vapor deposition. *physica status solidi (a)* **2016**, *213* (4), 1002−1009.
(41) Miller, R. F.; Taylor, A. J. Optical constants of thin films by an optimized reflection ratio method. *J. Phys. D: Appl. Phys.* **1971**, *4* (9), 1419.
(42) Brimhall, N.; Heilmann, N.; Ware, M.; Peatross, J. Polarization-ratio reflectance measurements in the extreme ultraviolet. *Opt. Lett.* **2009**, *34* (9), 1429−1431.
(43) Kranert, C.; Sturm, C.; Schmidt-grund, R.; Grundmann, M. Raman tensor elements of β-Ga2O3. *Sci. Rep.* **2016**, *6* (1), No. 35964.

https://doi.org/10.1021/acsomega.3c10280
ACS Omega 2024, 9, 27963−27968